

Absence of orbital current torque in Ta/ferromagnet bilayers

Qianbiao Liu,¹ Lijun Zhu^{1,2*}

¹ *Institute of Semiconductors, Chinese Academy of Sciences, Beijing 100083, China*

² *College of Materials Science and Opto-Electronic Technology, University of Chinese Academy of Sciences, Beijing 100049, China*

*ljzhu@semi.ac.cn

It has become a heated debate as to whether the orbital Hall effect of a material could generate a non-local orbital current and a non-zero spin-orbit torque on an adjacent magnetic layer. Here, we report unambiguous evidence that, regardless of the ferromagnets (FMs) (e.g., Ni, Ni₈₁Fe₁₉, Fe, Fe₆₀Co₂₀B₂₀, and FePt), the spin-orbit torque generated by an adjacent Ta, which is predicted to have a 50 times greater positive orbital Hall conductivity than the negative spin Hall conductivity, has essentially the same, negative efficiency, in agreement with the spin Hall effect of Ta being the only source of the interfacial torque. We identify that the constant, positive estimate of the torque of the Ta/FM samples from spin-torque ferromagnetic resonance (ST-FMR) analysis in a specific FM thickness range (≥ 2 nm for Ni), that was heavily cited in the literature to signify an orbital current torque but strongly disagrees with the fairly long relaxation length in other orbital current torque claims, results from the overlook of a significant thick-dependent self-induced ST-FMR signal of the FM. These results indicate the absence of orbital current torque in Ta/ferromagnet systems, regardless of the type, the SOC strength, and the layer thickness of the ferromagnets.

The development of fast, energy-efficient memory and computing technologies has triggered bloomed interest in the spin-orbit torques (SOTs) exerted on a ferromagnet (FM) by spin currents.^[1-3] Since the discovery of the SOTs,^[1,2] it had been a consensus that the spin currents associated with the SOTs are only *directly* generated by the spin Hall effect (SHE)^[1,3-8] or interfacial spin-orbit coupling (SOC) effects^[2,9-14] and that the orbital angular momentum is highly localized and gets completely quenched within a very short length scale of 0.2-0.4 nm, regardless of the SOC.^[15-17] Until very recently, some experiments,^[18-23] which cannot be readily understood by directly generated spin currents, together with some orbital current theories,^[24,25] stimulated searching for *indirect* sources of spin currents from orbital-to-spin conversion via a bulk or interfacial SOC (Fig. 1(a)).

Searching for hints for indirectly generating spin currents from the flow of orbital angular momentum has now become a rapidly growing interest in the field of spintronics^[26-40]. For the sake of convenience, below we use orbital current torque to rename the SOTs with an orbital current as the initial source of the spin current. However, to be precise, experiments cannot directly tell whether the measured SOTs are initially due to a spin or orbital current because orbital current cannot interact with magnetization until being converted into a spin current.

So far, the most likely observations that support the existence of orbital torque rely on the use of Ni as the torque detector.^[20,22,32-35] The dampinglike torque efficiency (ξ_{DL}^j) of Ta/Ni bilayers was analyzed, e.g., using spin-torque ferromagnetic resonance (ST-FMR), as positive in the Ni thickness range of a few nanometers, in striking contrast to the negative spin Hall ratio of Ta as measured using bilayers of Ta/non-Ni 3d FMs (e.g., Ni₈₁Fe₁₉, Fe, FeCoB).^[20,22] The argument from this observation in the literature was usually that Ni had a weak but slightly stronger SOC than Ni₈₁Fe₁₉, Co, Fe, and Fe₆₀Co₂₀B₂₀ such that Ni more efficiently converted the orbital current from Ta into spin current and generated a much stronger positive orbital torque than the negative spin Hall torque on the FM (the orbital Hall conductivity of Ta is predicted by band structure calculation to be

20-50 times greater than and of opposite sign compared to its spin Hall conductivity^[41,42]). To explain the different experiments, such orbital torque argument had to assume that the efficiency of orbital-spin conversion of a material or interface was proportional to its SOC strength and that the orbital relaxation length of the sputter-deposited polycrystalline Ni was less than 0.5 nm (as indicated by the constant SOT for Ni thicker than < 3 nm^[20], see the estimation of the relaxation rate in Fig. S1^[43]) or greater than 4 nm (as indicated by the continuous increase of the SOT with Ni thickness up to 20 nm^[32-34]). Following the similar arguments and with Ni as the detector, the generation of orbital current torque has been also claimed for many light metals that were believed to have little contribution to SOT generation before, such as Cr^[19,26,29] and Ti^[32,36]. Given the widespread impact and the striking disagreements between the orbital-current-torque arguments and the long-standing consensus and between different orbital torque arguments, careful experimental test of the in-depth physics and a unified, precise understanding of the Ta/ferromagnet are urgently required.

Here, we demonstrate evidence for the absence of orbital torque in the prototype Ta/FM systems, regardless of the type, the layer thickness, and the SOC of the FM. We find that the positive ξ_{DL}^j of the Ta/Ni, that is heavily cited in the literature as the most robust evidence of orbital torque, is a misinterpretation of a non-negligible self-induced ST-FMR signal of the FM layer.

We sputter-deposited in-plane magnetized Ta 5nm/FM bilayers with the FM of Ni, Ni₈₁Fe₁₉, Fe₆₀Co₂₀B₂₀, Fe, and FePt and several control samples specified below to study the SOTs generated by the SHE and the orbital Hall effect of Ta as a function of the type, the thickness (t_{FM}), and the SOC strength of the FM and the interface. Each bilayer is grown on an oxidized silicon substrate and protected by a MgO 2/Ta 2 bilayer (numbers are the layer thicknesses in nm) that is fully oxidized upon exposure to the atmosphere.^[44] These samples are patterned into ST-FMR microstrips with different aspect ratios by photolithography and ion milling, followed by deposition of contacts of Ti 5/Pt 150. The resistivity of the Ta layer is determined to be 200 $\mu\Omega$ cm.

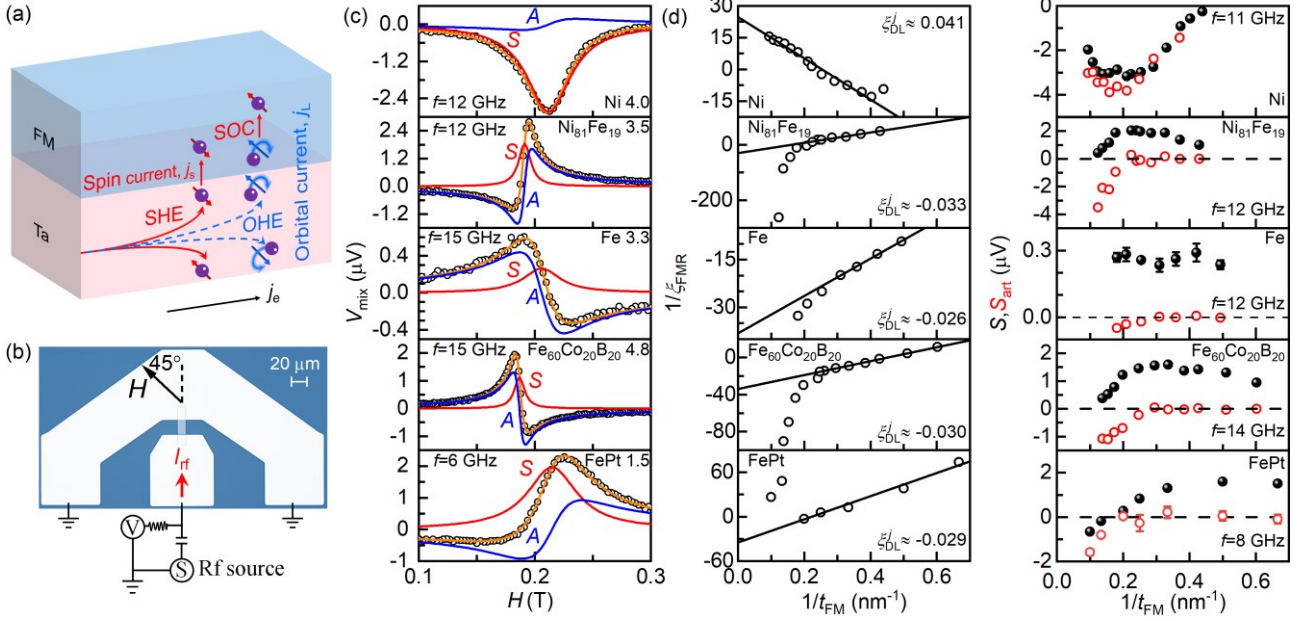


Fig. 1. ST-FMR analysis. (a) Schematic of potential torque generation in Ta/ferromagnet bilayer by the spin Hall effect and orbital Hall effect of Ta. (b) Optical microscopy image and measurement geometry of a ST-FMR device. (c) Typical ST-FMR spectra for Ta 5/Ni 4, Ta 5/Ni₈₁Fe₁₉ 3.5, Ta 5/Fe 3.3, Ta 5/Fe₆₀Co₂₀B₂₀ 4.8 ($\varphi = 45^\circ$, 12GHz), with the three solid curves plotting the best fit of the data to Eq. (1) (in orange), the symmetric (in red), and antisymmetric (in black) components. Inverse thickness dependence of (d) $1/\chi_{\text{FMR}}^j$ and (e) the total and artifact symmetric ST-FMR components (S and S_{art}) for the Ta/Ni, Ta/Ni₈₁Fe₁₉, Ta/Fe, Ta/Fe₆₀Co₂₀B₂₀, and Ta/FePt samples. Solid lines in (d) represent linear fits. In (e) S_{art} for Ni is measured from the Ni single-layer samples, while S_{art} for other samples is estimated from the deviation of the linear fit of $1/\chi_{\text{FMR}}^j$ vs $1/t_{\text{FM}}$ in (d). The rf power is 8 dBm.

We measure the SOTs of the Ta/FM using the three-terminal ST-FMR technique using the longitudinal voltage response (via magnetoresistance effects) by sweeping the in-plane magnetic field (H) at the azimuth angle (φ) of 45° relative to the rf current direction (Fig. 1b). As shown in Fig. 1c, each of the samples exhibits strong ST-FMR response (V_{mix}), fit of which to the relation [45]

$$V_{\text{mix}} = S \frac{\Delta H^2}{\Delta H^2 + (H - H_r)^2} + A \frac{\Delta H(H - H_r)}{\Delta H^2 + (H - H_r)^2}, \quad (1)$$

yields the magnitudes of the symmetric and antisymmetric components (S and A), the FMR linewidth (ΔH), and the resonance field (H_r). Since the $\sin 2\varphi \cos \varphi$ scaling of S and A (Fig. S2) have revealed no indication of any perpendicular spins [46] or perpendicular Oersted field [47], we define the ST-FMR efficiency (ζ_{FMR}^j) as

$$\zeta_{\text{FMR}}^j = \frac{S}{A} \frac{e \mu_0 M_s t_{\text{FM}} t_{\text{HM}}}{\hbar} \sqrt{1 + 4\pi M_{\text{eff}}/H_r}, \quad (2)$$

where e is the elementary charge, μ_0 the permeability of the vacuum, M_s the saturation magnetization of the FM, and \hbar the reduced Planck's constant. $4\pi M_{\text{eff}}$ is the effective demagnetization field of the FM and can be determined from the rf frequency (f) dependence of H_r following the Kittel's equation (Fig. S3a,b [43]). As shown in Fig. 1d, ξ_{DL}^j and the fieldlike torque efficiency (ξ_{FL}^j) can be estimated from the inverse intercept of the linear fit of $1/\chi_{\text{FMR}}^j$ vs $1/t_{\text{FM}}$ in the small-thickness regime following [5]

$$\frac{1}{\xi_{\text{FMR}}^j} = \frac{1}{\xi_{\text{DL}}^j} \left(1 + \frac{\hbar \xi_{\text{FL}}^j}{e \mu_0 M_s t_{\text{FM}} t_{\text{HM}}} \right). \quad (3)$$

So far, we have assumed that in the linear regime S and A

included only negligible “artifacts” contributions (S_{art} , A_{art}) from spin pumping ($S_{\text{art}} \neq 0$, $A_{\text{art}} = 0$) [46,48–50], the anomalous Nernst effect (due to a vertical thermal gradient formed by the unbalanced thermal dissipation at the substrate and the surface, $S_{\text{art}} \neq 0$, $A_{\text{art}} = 0$) [51], and bulk SOT ($S_{\text{art}} \neq 0$, $A_{\text{art}} \neq 0$) [44]. These contributions, if significant, may induce deviation from the linear scaling typically in the thick limit (see data of the Ni₈₁Fe₁₉, Fe, Fe₆₀Co₂₀B₂₀, and FePt samples in Fig. 1d,e).

As summarized in Fig. 2a, the ξ_{DL}^j values estimated from the above linear-regime analyses remain essentially the same for the Ta/Ni₈₁Fe₁₉ (-0.033 ± 0.004), the Ta/Fe₆₀Co₂₀B₂₀ (-0.030 ± 0.004), the Ta/Fe (-0.026 ± 0.001), and the Ta/FePt (-0.029 ± 0.005). This result suggests a constant ξ_{DL}^j for the Ta/FM bilayer with the FM thickness within the linear regime (typically <4–5 nm). In contrast, ξ_{DL}^j for the Ta/Ni is estimated to be $+0.041 \pm 0.003$, which is of much higher magnitude and opposite sign compared to others. Such positive estimate for ξ_{DL}^j of Ta/Ni was cited as the key evidence for the presence of a strong orbital current torque in previous reports [19,20,22]. The positive, constant ξ_{DL}^j estimate at the Ni thicknesses of ≥ 2.5 nm, if represented an orbital current torque, would require the relaxation length of the associated spin and orbital currents to be as short as <0.5 nm (Fig. S1 [43]), which strongly disagrees with the fairly long relaxation length of nonmagnetic and magnetic metals in some orbital current torque claims [19,26,29,32–34].

Since the bulk SOC of the FM is approximately a linear function of the composition [52], we estimate the bulk SOC strength as 107 meV for Ni, 99 meV for Ni₈₁Fe₁₉, 70 meV for Fe, 59 meV for Fe₆₀Co₂₀B₂₀, and

335 meV for FePt (Fig. 2b), using the elemental SOC strengths [53]. The SOC of Ni is only very slightly greater than that of Ni₈₁Fe₁₉, Fe, and Fe₆₀Co₂₀B₂₀, but 3 times weaker than that of FePt. The nonlocal orbital current assumption must predict a very strong orbital torque in Ta/FePt with both a giant orbital Hall conductivity in Ta and a strong SOC in FePt but a considerably weak one in Ta/Ni, Ta/Ni₈₁Fe₁₉, Ta/Fe, and Ta/Fe₆₀Co₂₀B₂₀ samples. The bulk SOC is unlikely to make Ni so different from the other FMs, including Ni₈₁Fe₁₉, 81% of which is also Ni. Thus, the FM type dependence disproves the bulk SOC as the cause of the positive ξ_{DL}^j value for the Ta/Ni. Figure 2c shows the magnetic anisotropy energy density (K_s) of the FM interfaces as the indicator of the interfacial SOC [54,55]. Except for the Fe sample with strong SOC at the Fe/MgO and Ta/Fe interfaces, all the other samples have minimal interfacial SOC at the FM interfaces. While the strong interfacial SOC for the Fe samples explains the slightly smaller ξ_{DL}^j than others because the enhanced interfacial SOC of the Ta/Fe interface should decrease the spin transparency of the interface vis spin memory loss [8,54], the positive estimate of ξ_{DL}^j for the Ni sample cannot be attributed to any role of the interfacial SOC. Therefore, these observations consistently reveal the absence of orbital torque in all the Ta/FM samples.

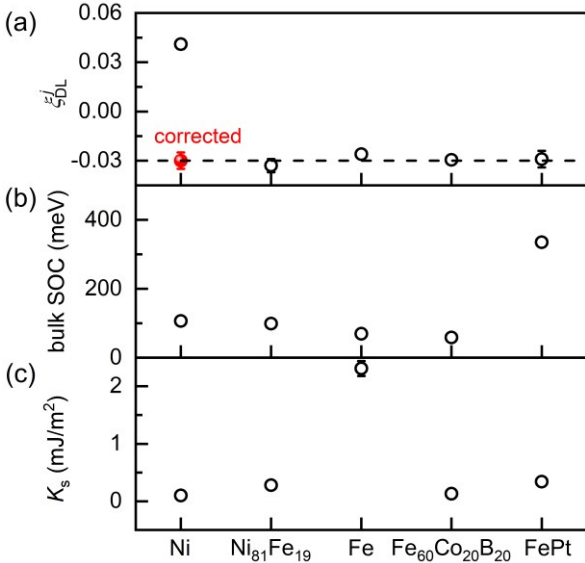


Fig. 2. Absence of orbital current torque. (a) Efficiency of the dampinglike spin-orbit torque, (b) bulk SOC strength, and (c) Sum interfacial magnetic anisotropy energy density of the magnetic interfaces for the Ta/FM bilayers plotted as a function of the FM type.

We discuss below that the positive torque estimate is most likely induced by the presence of a significant thickness-dependent self-induced bulk SOT within the FM layers. We have measured S_{art} and A_{art} signals (from the control devices of single-layer Ni) that are rather significant compared to the total S and A signals of the Ta/Ni bilayer devices (see Fig. 1e and Fig. S4 [43] for S_{art} vs S and A_{art} vs A), suggesting the presence of a strong self-induced ST-FMR in the Ni layer in the thickness range of >2 nm. The Ta/Ni₈₁Fe₁₉, Ta/Fe, Ta/Fe₆₀Co₂₀B₂₀, and Ta/FePt samples also demonstrate a deviation from

linear scaling in the thick limit (typically > 4-5 nm, Fig. 1d). These observations are consistent with the previous reports of self-induced bulk SOT in magnetic single layers, e.g., CoPt [44], Ni₈₁Fe₁₉ [56], Fe₆₀Co₂₀B₂₀ [57], FePt [58], and Fe_xTb_{1-x} [59]. The emergence only beyond a non-zero threshold layer thickness is also a typical characteristic of the bulk SOT effect [44]. While the torque contribution from the Ta layer cannot be directly estimated from a linear dependence of $1/\zeta_{FMR}$ vs $1/t_{FM}$ due to the thickness-dependent bulk SOT contribution in the available thickness range in Fig. 1d, the true S and A contributions of the Ta layer can be estimated by subtracting the bulk SOT contributions (calibrated from the single Ni layer whose conductance is a factor of ~ 10 greater than the 5 nm Ta such that the rf current with the Ni layers is reasonably close for the Ta/Ni sample and the control Ni single-layer sample) from the total S and A contributions of the Ta/Ni. With the true values of S and A contributed by the Ta layer, we calculate ζ_{FMR} of the Ta/Ni devices with different Ni thicknesses following Eq. (2). As shown in Fig. 3a, the linear fit of $1/\zeta_{FMR}$ vs $1/t_{Ni}$ for the Ta/Ni yields a constant dampinglike torque efficiency of -0.030 ± 0.005 (the red solid dot in Fig. 2a) for the Ni thickness range from 2 nm to 10 nm, which coincides well with that of non-Ni samples.

We also note that the positive estimate of ξ_{DL}^j or S_{art} in the particularly wide-thickness range for the Ni samples (Fig. 1e) cannot be explained by any pumping of spin or orbital current from the FM into the Ta. The contribution of spin/orbital pumping to S_{art} via the inverse SHE of Ta should decrease upon enhancement of the conductivity, magnetic damping, and magnetization of the FM [51]. However, the Ni has the highest conductivity (lowest resistivity) and the highest damping among the studied FMs and similar magnetization as the FePt (Fig. 3b and Fig. S3c [43]). This is consistent with the previous estimation of negligible spin pumping contribution to the ST-FMR signal in the Ta and Pt devices in the pioneering works [1,45].

To test any anomalous Nernst voltage effect, we fabricated ST-FMR devices with a 150 nm Si₃N₄ on the top of the Ta/Ni microstrips (Fig. 3c). The thick, high thermal-conductivity [60] Si₃N₄ layer is expected to lower or even reverse the rf-heating-induced vertical thermal gradient, if any. However, the $1/\zeta_{FMR}$ vs $1/t_{Ni}$ data of these devices still yields a similar positive estimate of $\xi_{DL}^j \approx 0.055$ for the Ta/Ni (Fig. 3c), which is close to that of the devices without any top Si₃N₄ sink layer (Fig. 1d). ζ_{FMR} also shows little enhancement as the rf power is increased from 0.01 dBm to 15 dBm (Fig. 3d). The same sign of S_{art} for samples with different types of FMs (Fig. 1e) disagrees the opposite signs of the anomalous Nernst coefficient of thick Fe and Ni or Ni₈₁Fe₁₉ [61,62,63]. The anomalous Nernst effect cannot explain the presence of non-zero A_{art} signals in Ni single layers (Fig. S4 [43]) and the similar deviation trend from the linear scaling of $1/\zeta_{FMR}$ vs $1/t_{Ni}$ for the Pt/Co and the Co/Pt devices in our previous experiments [50]. Thus, the anomalous Nernst voltage can be safely excluded as the cause of the deviation from the linear scaling of $1/\zeta_{FMR}$ vs $1/t_{Ni}$ in Fig. 1d and the positive estimate of ξ_{DL}^j for the Ta/Ni samples. These results reveal that the true dampinglike

SOT of the Ta/FM samples is always negative, regardless of the type, the SOC strength, and the thickness of the FM. This also reaffirms that the orbital Hall effect, which is 50 times greater than the SHE in Ta in theory [41,42], makes no detectable contribution to the SOT on the FM layer.

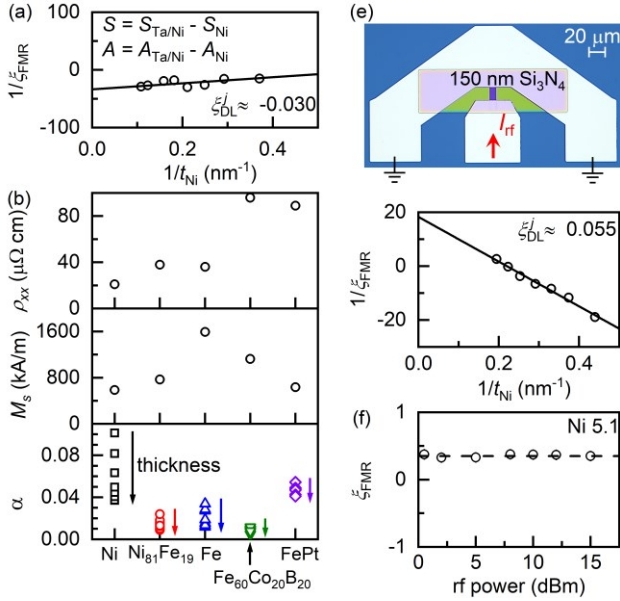


Fig. 3. Origin of the positive estimate of the SOT for the Ta/Ni devices. (a) Linear scaling of the corrected $1/\zeta_{\text{FMR}}$ with $1/t_{\text{FM}}$, indicating a dampinglike torque efficiency of -0.030 ± 0.005 . (b) Resistivity, Magnetization, and Magnetic damping of the Ta/FM bilayers with different FM thicknesses. (c) Optical microscopy image and $1/\zeta_{\text{FMR}}$ vs $1/t_{\text{FM}}$ for the Ta/Ni devices with a 150 nm Si₃N₄ thermal sink on the top. (d) Minimal variation of ζ_{FMR} with the rf power for Ta 5/Ni 5.1. The solid lines in (a) and (c) plot the linear fits, while the dashed line in (d) is to guide the eyes.

In summary, we have established robust evidence for the absence of orbital current torque in the Ta/FM bilayers, regardless of the type, the SOC strength, and the layer thickness of the FM. These findings have clarified the heated debate over the orbital current torque and have indicated a critical need to recheck the reported orbital current torque in samples containing Ni or other FMs with self-induced ST-FMR signals. Given the blooming interest, further efforts are also required to address the essential challenges on the orbital current torque in light metal/FM systems. For example, the argument that Ti generated strong non-local orbital current [31-33] is not supported by our previous experimental observation of minimal torque generation in Ti/FM bilayers with very strong interfacial SOC [64]. The arguments of a non-local orbital current and an orbital relaxation length of >70 nm in Ti [31,32] are strongly challenged by recent first-principles quantum mechanical scattering calculations that orbital angular momentum always gets completely relaxed within 1-2 atomic scales regardless of the SOC [17] and by the classical orbital quenching arguments [15,16]. The claims of giant torque on the FM due to orbital-spin conversion in Pt within TmIG/Pt 1.5/CuO_x [18], Mn/Pt 1-6/Co [37], Py/Pt 4/CuO_x [38], YIG/Pt 2/CuO_x [39], and Co/Pt 4/Cu [65] are not consistent with the

previous experiments that the spin diffusion length of 1 nm or less for very thin, resistive Pt with enhanced interfacial electron scattering [66]. The argument of efficient orbital-spin conversion in Pt in the FM/Pt/orbital-source material trilayers [18,37-39,65] must require a very short orbital relaxation length for Pt, which strongly disagrees with the very long orbital diffusion length suggested by the torque results even at the Pt thickness of >12.5 nm in the ST-FMR analysis and of >85 nm in the magneto-optical detection [33]. Our recent study [67] has revealed that the spin-Hall-magnetoresistance-like behaviors in magnetic heterostructures without a heavy metal, which were claimed to support orbital angular momentum effect [23,29,68], can be attributed simply to electron scattering by the magnetization and interfacial electric field within the two-vector magnetoresistance frame [69], without relevance to any spin or orbital angular momentum. The enhanced perpendicular effective field in FM/Pt/Ta or Cu [28] could be attributed to a Pt-enhanced perpendicular intralayer Dzyaloshinskii-Moriya interaction field [70] and thus cannot signify the enhanced orbit-spin conversion in Pt. Care is also needed in the discussion of orbital current from THz emission that can include a strong contribution from the anomalous Nernst effect, and the sign of the latter can vary as a function of the type and thickness of the FMs [62,63,71]. The universal deviation from the linear scaling of $1/\zeta_{\text{FMR}}$ vs $1/t_{\text{FM}}$ suggests that the widely adopted ST-FMR analysis of dampinglike SOT of a magnetic heterostructures using a single sample is highly unreliable even when the magnetic layer was very thick (>10 nm) such that the fieldlike SOT contribution became weak.

Acknowledgments

This work is supported partly by the Beijing National Natural Science Foundation (Z230006), the National Key Research and Development Program of China (2022YFA1204000), and by the National Natural Science Foundation of China (12304155, 12274405).

Author contribution

L.Z. conceived the project, Q. L. fabricated the samples and performed the transport measurements, L. Z. and Q. L. wrote the manuscript.

Competing interests: The authors declare no competing interests.

Correspondence and requests for materials should be addressed to Lijun Zhu.

- [1] L. Liu, C.-F. Pai, Y. Li, H. W. Tseng, D. C. Ralph, and R. A. Buhrman, Spin-torque switching with the giant spin Hall effect of tantalum, *Science* **336**, 555 (2012).
- [2] I. M. Miron, K. Garello, G. Gaudin, P.-J. Zermatten, M. V. Costache, S. Auffret, S. Bandiera, B. Rodmacq, A. Schuhl, and P. Gambardella, Perpendicular switching of a single ferromagnetic layer induced by in-plane current injection. *Nature (London)* **476**, 189 (2011).
- [3] L. Zhu, Switching of Perpendicular Magnetization by Spin-Orbit Torque. *Adv. Mater.* **35**, 2300853 (2023).
- [4] P. M. Haney, H. W. Lee, K. J. Lee, A. Manchon, and M. D. Stiles, Current induced torques and interfacial spin-orbit coupling: Semiclassical modeling. *Phys. Rev. B* **87**, 174411 (2013).

- [5] C. Pai, Y. Ou, L. H. Vilela-Leão, D. C. Ralph, and R. A. Buhrman, Dependence of the efficiency of spin Hall torque on the transparency of Pt/ferromagnetic layer interfaces, *Phys. Rev. B* **92**, 064426 (2015).
- [6] L. Zhu, L. Zhu, M. L. Sui, D. C. Ralph, and R. A. Buhrman, Variation of the giant intrinsic spin Hall conductivity of Pt with carrier lifetime. *Sci. Adv.* **5**, eaav8025 (2019).
- [7] L. Zhu, D. C. Ralph, R. A. Buhrman, Maximizing spin-orbit torque generated by the spin Hall effect of Pt, *Appl. Phys. Rev.* **8**, 031308 (2021).
- [8] Y. Liu, Z. Yuan, R. J. H. Wesselink, A. A. Starikov, and P. J. Kelly, Interface Enhancement of Gilbert Damping from First Principles, *Phys. Rev. Lett.* **113**, 207202 (2014).
- [9] V. P. Amin, J. Zemen, and M. D. Stiles, Interface-Generated Spin Currents, *Phys. Rev. Lett.* **121**, 136805 (2018).
- [10] L. Wang, R. J. H. Wesselink, Y. Liu, Z. Yuan, K. Xia, and P. J. Kelly, Giant Room Temperature Interface Spin Hall and Inverse Spin Hall Effects, *Phys. Rev. Lett.* **116**, 196602 (2016).
- [11] S. Li, K. Shen, and K. Xia, Interfacial spin Hall effect and spin swapping in Fe-Au bilayers from first principles, *Phys. Rev. B* **99**, 134427 (2019).
- [12] K.-W. Kim, K.-J. Lee, J. Sinova, H.-W. Lee, and M. D. Stiles, Spin-orbit torques from interfacial spin-orbit coupling for various interfaces, *Phys. Rev. B* **96**, 104438 (2016).
- [13] X. Wang and A. Manchon, Diffusive Spin Dynamics in Ferromagnetic Thin Films with a Rashba Interaction, *Phys. Rev. Lett.* **108**, 117201 (2012).
- [14] P. M. Haney, H.-W. Lee, K.-J. Lee, A. Manchon, and M. D. Stiles, Current induced torques and interfacial spin-orbit coupling: Semiclassical modeling, *Phys. Rev. B* **87**, 174411 (2013).
- [15] P. Mohn, in *Magnetism in the Solid State: An Introduction*, edited by M. Cardona, P. Fulde, K. von Klitzing, and H.-J. Queisser, Springer Series in Solid-State Sciences (Springer, Berlin, Heidelberg, 2003), Vol. 134.
- [16] M. Tinkham, *Group Theory and Quantum Mechanics*, Dover Books on Chemistry (Dover, New York, 2003).
- [17] M. Rang and P. J. Kelly, Orbital relaxation length from first-principles scattering calculations, *Phys. Rev. B* **109**, 214427 (2024).
- [18] S. Ding, A. Ross, D. Go, L. Baldrati, Z. Ren, F. Freimuth, S. Becker, F. Kammerbauer, J. Yang, G. Jakob, Y. Mokrousov, and M. Kläui, Harnessing Orbital-to-Spin Conversion of Interfacial Orbital Currents for Efficient Spin-Orbit Torques, *Phys. Rev. Lett.* **125**, 177201 (2020).
- [19] S. Lee, M. Kang, D. Go, D. Kim, J. Kang, T. Lee, G. Lee, J. Kang, N. J. Lee, Y. Mokrousov, S. Kim, K. Kim, K. Lee, and B. Park, Efficient conversion of orbital Hall current to spin current for spin-orbit torque switching. *Commun. Phys.* **4**, 234 (2021).
- [20] D. Lee, D. Go, H. Park, W. Jeong, H. Ko, D. Yun, D. Jo, S. Lee, G. Go, J. H. Oh, K. Kim, B. Park, B. Min, H. C. Koo, H. Lee, O. Lee, and K. Lee, Orbital torque in magnetic bilayers, *Nat. Commun.* **12**, 6710 (2021).
- [21] J. Kim, D. Go, H. Tsai, D. Jo, K. Kondou, H. Lee, and Y. Otani, Nontrivial torque generation by orbital angular momentum injection in ferromagnetic-metal/Cu/Al₂O₃ trilayers, *Phys. Rev. B* **103**, L020407 (2021).
- [22] S. Dutta and A. A. Tulapurkar, Observation of nonlocal orbital transport and sign reversal of dampinglike torque in Nb/Ni and Ta/Ni bilayers, *Phys. Rev. B* **106**, 184406 (2022).
- [23] S. Ding, Z. Liang, D. Go, C. Yun, M. Xue, Z. Liu, S. Becker, W. Yang, H. Du, C. Wang, Y. Yang, G. Jakob, M. Kläui, Y. Mokrousov, and J. Yang, Observation of the Orbital Rashba-Edelstein Magnetoresistance. *Phys. Rev. Lett.* **128**, 067201 (2022).
- [24] D. Go, D. Jo, C. Kim, and H. Lee, Intrinsic Spin and Orbital Hall Effects from Orbital Texture, *Phys. Rev. Lett.* **121**, 086602 (2018).
- [25] D. Jo, D. Go, H.-W. Lee, Gigantic intrinsic orbital Hall effects in weakly spin-orbit coupled metals. *Phys. Rev. B* **98**, 214405 (2018).
- [26] G. Sala and P. Gambardella, Giant orbital Hall effect and orbital-to-spin conversion in 3d, 5d, and 4f metallic heterostructures, *Phys. Rev. Res.* **4**, 033037 (2022).
- [27] A. Bose, F. Kammerbauer, R. Gupta, D. Go, Y. Mokrousov, G. Jakob, and M. Kläui, Detection of long-range orbital-Hall torques. *Phys. Rev. B* **107**, 134423 (2023).
- [28] T. Li, L. Liu, X. Li, X. Zhao, H. An, and K. Ando, Giant Orbital-to-Spin Conversion for Efficient Current-Induced Magnetization Switching of Ferrimagnetic Insulator. *Nano Lett.* **23**, 7174 (2023).
- [29] H. Xie, N. Zhang, Y. Ma, X. Chen, L. Ke, Y. Wu, Efficient Noncollinear Antiferromagnetic State Switching Induced by the Orbital Hall Effect in Chromium, *Nano Lett.* **23**, 10274 (2023).
- [30] I. Lyalin, S. Alikhah, M. Berritta, P. M. Oppeneer, and R. K. Kawakami, Magneto-Optical Detection of the Orbital Hall Effect in Chromium, *Phys. Rev. Lett.* **131**, 156702 (2023).
- [31] Y.-G. Choi, D. Jo, K.-H. Ko, D. Go, K.-H. Kim, H. G. Park, C. Kim, B.-C. Min, G.-M. Choi, H.-W. Lee, Observation of the orbital Hall effect in a light metal Ti. *Nature* **619**, 52 (2023).
- [32] H. Hayashi, D. Jo, D. Go, T. Gao, S. Haku, Y. Mokrousov, H.-W. Lee, K. Ando, Observation of long-range orbital transport and giant orbital torque. *Commun. Phys.* **6**, 32 (2023).
- [33] H. Moriya, M. Taniguchi, D. Jo, D. Go, N. Soya, H. Hayashi, Y. Mokrousov, H. Lee, and K. Ando, Observation of Long-Range Current-Induced Torque in Ni/Pt Bilayers, *Nano Lett.* **24**, 6459 (2024).
- [34] R. Fukunaga, S. Haku, H. Hayashi, K. Ando, Orbital torque originating from orbital Hall effect in Zr. *Phys. Rev. Res.* **5**, 023054 (2023).
- [35] R. Fukunaga, S. Haku, T. Gao, H. Hayashi, and K. Ando, Impact of crystallinity on orbital torque generation in ferromagnets, *Phys. Rev. B* **109**, 144412 (2024).
- [36] H. Hayashi, D. Go, S. Haku, Y. Mokrousov, K. Ando, Observation of orbital pumping, *Nat. Electron.* **7**, 646 (2024).
- [37] Z. Zheng, T. Zeng, T. Zhao, S. Shi, L. Ren, T. Zhang, L. Jia, Y. Gu, R. Xiao, H. Zhou, Q. Zhang, J. Lu, G. Wang, C. Zhao, H. Li, B. K. Tay, and J. Chen, Effective electrical manipulation of a topological antiferromagnet by orbital torques. *Nat. Commun.* **15**, 745 (2024).
- [38] E. Santos, J. E. Abrão, A. S. Vieira, J. B. S. Mendes, R. L. Rodríguez-Suárez, and A. Azevedo, Exploring orbital-charge conversion mediated by interfaces with CuO_x through spin-orbital pumping. *Phys. Rev. B* **109**, 014420 (2024).

- [39] J. A. Mendoza-Rodarte, M. Cosset-Chéneau, B. J. van Wees, and M. H. D. Guimarães, Efficient Magnon Injection and Detection via the Orbital Rashba-Edelstein Effect, *Phys. Rev. Lett.* 132, 226704 (2024).
- [40] S. Ding, M. Kang, W. Legrand, and P. Gambardella, Orbital Torque in Rare-Earth Transition-Metal Ferrimagnets, *Phys. Rev. Lett.* 132, 236702 (2024).
- [41] T. Tanaka, H. Kontani, M. Naito, T. Naito, D. S. Hirashima, K. Yamada, J. Inoue, Intrinsic spin Hall effect and orbital Hall effect in 4d and 5d transition metals. *Phys. Rev. B* 77, 165117 (2008).
- [42] H. Kontani, T. Tanaka, D. S. Hirashima, K. Yamada, and J. Inoue, Giant Orbital Hall Effect in Transition Metals: Origin of Large Spin and Anomalous Hall Effects. *Phys. Rev. Lett.* 102, 016601 (2009).
- [43] See the Supplementary Materials for more information on Estimation of the relaxation length of angular momentum, Angle-dependent ST-FMR analysis, More sample parameters as determined from the ST-FMR measurements, Spin pumping of y spins during the ST-FMR analysis, and Antisymmetric ST-FMR signals of the Ta/Ni and Ni samples.
- [44] L. Zhu, X. S. Zhang, D. A. Muller, D. C. Ralph, R. A. Buhrman, Observation of strong bulk damping-like spin-orbit torque in chemically disordered ferromagnetic single layers, *Adv. Funct. Mater.* 30, 2005201 (2020).
- [45] L. Liu, T. Moriyama, D. C. Ralph, R. A. Buhrman, Spin-torque ferromagnetic resonance induced by the spin Hall effect, *Phys. Rev. Lett.* 106, 036601 (2011).
- [46] Q. Liu, X. Lin, A. Shaked, Z. Nie, G. Yu, and L. Zhu, Efficient Generation of Out-of-Plane Polarized Spin Current in Polycrystalline Heavy Metal Devices with Broken Electric Symmetries. *Adv. Mater.* 36, 2406552 (2024).
- [47] Q. Liu, L. Zhu, Current-induced perpendicular effective magnetic field in magnetic heterostructures. *Appl. Phys. Rev.* 9, 041401(2022).
- [48] H. Nakayama, K. Ando, K. Harii, T. Yoshino, R. Takahashi, Y. Kajiwara, K. Uchida, Y. Fujikawa, and E. Saitoh, Geometry dependence on inverse spin Hall effect induced by spin pumping in $\text{Ni}_{81}\text{Fe}_{19}/\text{Pt}$ films, *Phys. Rev. B* 85, 144408 (2012).
- [49] O. Mosendz, V. Vlaminck, J. E. Pearson, F. Y. Fradin, G. E. W. Bauer, S. D. Bader, A. Hoffmann, Detection and quantification of inverse spin Hall effect from spin pumping in permalloy/normal metal bilayers. *Phys. Rev. B* 82, 214403 (2010).
- [50] L. Zhu, L. Zhu, D.C. Ralph, and R.A. Buhrman, Origin of Strong Two-Magnon Scattering in Heavy-Metal/Ferromagnet/Oxide Heterostructures, *Phys. Rev. Appl.* 13, 034038 (2020).
- [51] S. Karimeddiny, J. A. Mittelstaedt, R. A. Buhrman, D. C. Ralph, Transverse and longitudinal spin-torque ferromagnetic resonance for improved measurement of spin-orbit torque, *Phys. Rev. Appl.* 14, 024024 (2020).
- [52] D. Kim and F. Liu, Topological alloy engineering and locally linearized gap dependence on concentration, *Phys. Rev. B* 106, 085105 (2022).
- [53] K. V. Shanavas, Z. S. Popovic, and S. Satpathy, Theoretical model for Rashba spin-orbit interaction in d electrons, *Phys. Rev. B* 90, 165108 (2014).
- [54] L. Zhu, D. C. Ralph, R. A. Buhrman, Spin-orbit torques in heavy-metal-ferromagnet bilayers with varying strengths of interfacial spin-orbit coupling. *Phys. Rev. Lett.* 122, 077201 (2019).
- [55] L. Zhu, D. C. Ralph, R. A. Buhrman, Effective spin-mixing conductance of heavy metal ferromagnet interfaces. *Phys. Rev. Lett.* 123, 057203 (2019).
- [56] T. Seki, Y. Lau, S. Iihama, and K. Takanashi, Spin-orbit torque in a Ni-Fe single layer, *Phys. Rev. B* 104, 094430 (2021).
- [57] Y. Du, R. Thompson, M. Kohda, and J. Nitta, Origin of spin-orbit torque in single-layer CoFeB investigated via in-plane harmonic Hall measurements, *AIP Advances* 11, 025033 (2021).
- [58] L. Zhu, D. C. Ralph, R. A. Buhrman, Unveiling the mechanism of bulk spin-orbit torques within chemically disordered $\text{Fe}_x\text{Pt}_{1-x}$ single layers, *Adv. Funct. Mater.* 31, 2103898 (2021).
- [59] Q. Liu, L. Zhu, X. S. Zhang, D.A. Muller, D.C. Ralph, Giant bulk spin-orbit torque and efficient electrical switching in single ferrimagnetic FeTb layers with strong perpendicular magnetic anisotropy, *Appl. Phys. Rev.* 9, 021402 (2022).
- [60] H. Zhou, T. Feng, Theoretical upper limits of the thermal conductivity of Si_3N_4 , *Appl. Phys. Lett.* 122, 182203 (2023).
- [61] A. W. Smith, The Hall Effect and the Nernst Effect in Magnetic Alloys, *Phys. Rev.* 17, 23 (1921).
- [62] H. Zhang, et al., Tuning terahertz emission generated by anomalous Nernst effect in ferromagnetic metal, *Appl. Phys. Rev.* 10, 021417 (2023).
- [63] T. C. Chuang, P. L. Su, P. H. Wu, and S. Y. Huang, Enhancement of the anomalous Nernst effect in ferromagnetic thin films, *Phys. Rev. B* 96, 174406 (2017).
- [64] L. Zhu and R. A. Buhrman, Absence of significant spin current generation in Ti/FeCoB bilayers with strong interfacial spin-orbit coupling, *Phys. Rev. Appl.* 15, L031001 (2021).
- [65] S. Krishnia et al., Quantifying the large contribution from orbital Rashba-Edelstein effect to the effective damping-like torque on magnetization. *APL Mater.* 12, 051105 (2024).
- [66] M.-H. Nguyen, D. C. Ralph, and R. A. Buhrman, Spin Torque Study of the Spin Hall Conductivity and Spin Diffusion Length in Platinum Thin Films with Varying Resistivity, *Phys. Rev. Lett.* 116, 126601 (2016).
- [67] L. Zhu, Q. Liu, X. Wang, Physics origin of universal unusual magnetoresistance, unpublished.
- [68] H. Hayashi, K. Ando, Orbital Hall magnetoresistance in Ni/Ti bilayers, *Appl. Phys. Lett.* 123, 172401 (2023).
- [69] X. R. Wang, C. Wang, X. S. Wang, A theory of unusual anisotropic magnetoresistance in bilayer heterostructures, *Sci. Rep.* 13, 309 (2023).
- [70] Q. Liu, L. Liu, G. Xing, L. Zhu, Asymmetric magnetization switching and programmable complete Boolean logic enabled by long-range intralayer Dzyaloshinskii-Moriya interaction, *Nat. Commun.* 15, 2978 (2024).
- [71] Z. Feng, W. Tan, Z. Jin, Y.-J. Chen, Z. Zhong, L. Zhang, S. Sun, J. Tang, Y. Jiang, P.-H. Wu, J. Cheng, B. Miao, H. Ding, D. Wang, Y. Zhu, L. Guo, S. Shin, G.-H. Ma, D. Hou, and S.-Y. Huang, Anomalous Nernst Effect Induced Terahertz Emission in a Single Ferromagnetic Film, *Nano Lett.* 23, 8171 (2023).